Femtosecond laser micromilling of Si wafers

Lee, Seongkuk; Yang, Dongfang; Nikumb, Suwas

Publisher's version / Version de l'éditeur:
https://doi.org/10.1016/j.apsusc.2007.10.063
Applied Surface Science, 254, 10, pp. 2996-3005, 2008-03-15

Femtosecond Laser Micromilling of Si Wafers

Seongkuk Lee, Dongfang Yang, Suwas Nikumb

Integrated Manufacturing Technology Institute, National Research Council

800 Collip Circle, London, Ontario, Canada N6G 4X8

Abstract : Femtosecond laser micromilling of silicon is investigated using a regeneratively amplified 775 nm Ti:Sapphire laser with a pulse duration of 150 fs operating at 1 kHz repetition rate. The morphological observation and topological analysis of craters fabricated by single-shot laser irradiation indicated that the material removal is thermal in nature and there are two distinct ablation regimes of low fluence and higher fluence with logarithmical relations between the ablation depth and the laser fluence. Crater patterns were categorized into four characteristic groups and their formation mechanisms were investigated. Femtosecond laser micromilling of pockets in silicon was performed. The effect of process parameters such as pulse energy, translation speed, and the number of passes on the material removal rate and the formation of cone-shaped microstructures was investigated. The results indicate that the microstructuring mechanism has a strong dependence on the polarization, the number of passes and laser fluence. The optimal laser fluence range for Si micromilling was found to be 2~8 J/cm^2 and the milling efficiency attains its maximum between 10 ~ 20 J/cm^2.

PACS: 42.62.Cf; 79.20Ds; 81.20.Wk

Keywords: Femtosecond laser; Ablation; Micromilling; Silicon

1. Introduction

Laser-based machining of materials with femtosecond laser pulses has attracted considerable attention in recent years [1]. The reduction of temporal width of pulses from the nanosecond to the femtosecond regime limits the thermal diffusion into the surrounding material during ablation process and increases the quality of the machined surface [2]. In contrast to material processing using nanosecond or longer laser pulses where standard modes of thermal processes dominate, the case of femtosecond laser-material interactions, only a small fraction of the laser pulse energy is transmitted to the material surrounding the laser-irradiated area in the form of heat. Consequently, femtosecond laser pulses can induce nonthermal structural changes, driven by electronic excitation and associated nonlinear processes, before the material lattice attains equilibrium with the excited carriers. This fast mode of material modification process can reduce the thermal stresses significantly with minimal collateral damage of the processing materials [3].

Silicon is an important material in semiconductor industry and also very useful for MEMS devices. Femtosecond laser ablation of silicon has received significant attention mainly because of its potential in micromachining application [4]. Most of the studies in literature are focused on the physics of the transient states of the single pulse ablation process using techniques including optical pump-probe [5], time-of-flight mass spectroscopy [6-9], and time-resolved microscopy [10]. A number of theoretical models based on molecular dynamics have been proposed to model ultrafast heating and ablation processes [11-13]. Recently, the formation of microstructures (ripples, columns and cones) on Si samples in the case of multiple pulse irradiations on stationary samples has

been reported by several research groups [14-18]. Hwang et al [19] investigated the ablation process efficiency during silicon micromachining with femtosecond laser pulses in ambient air, and reported that the decrease of the ablation efficiency in the high fluence region (> 10 J/cm^2) is attributed to the strong interaction of the laser pulse with the laser-induced plasma. Crawford et al [20] carried out femtosecond laser micromachining of grooves in silicon and investigated ablation rate as a function of pulse energy, translation speed, and the number of consecutive passes. Coyne et al [21] analyzed the interaction of ultra-short pulses with wafer grade silicon in air using optical and electron microscope, and suggested that the optimum fluence condition for precise and accurate machining of silicon is in the range of 0.8 ~ 1.5 J/cm^2.

Laser micromilling is gradually emerging as an important technology for applications in material manufacturing, rapid prototyping and component miniaturization. It makes manufacturing cheaper, faster, cleaner and more accurate. This benefits product development by reducing risk and time to market, thereby increasing product competitiveness, improving performance and reliability [22,23]. In particular, laser micromilling permits a wide variety of structures in silicon since the process is independent of the crystal plane orientation unlike wet chemical etching process. Several research groups have investigated femtosecond laser micromachining of basic geometric features on a variety of materials such as borosilicate glass, silicon [16], fused silica [24,25], aluminum [25], copper [26], Lithium Niobate [27], Nitinol [28], PZT [29]. However, in comparison to nanosecond and picosecond lasers, relatively few systematic studies have been performed on the development of linear features in solid materials with femtoseocnd lasers.

The objective of the work reported in this paper is to characterize the ablation and micromilling of silicon using femtosecond laser pulses. First, single-shot laser experiments were carried out to create craters in silicon with the variation of laser fluence. Surface morphologies and topographies of the machined craters were obtained by field emission scanning electron microscopy and an optical surface profiler (WYKO, NT1100). The evolution of surface morphology, profiles of the craters and the ablation rates were investigated as a function of the laser fluence. Next, the femtosecond laser micromilling of shallow pockets in silicon was performed. Effects of the process parameters such as pulse energy, translation speed, and the number of passes on the material removal and the formation of microfeatures were studied in order to understand the characteristics and the parametric relationships of the laser micromilling process and to explore its application feasibility.

2. Experimental

The present experimental studies focus on the surface morphology of microfeatures (craters and pockets) created in silicon using single and multiple femtosecond laser pulses. A regeneratively amplified 775 nm Ti:Sapphire laser system (CPA-2010, Clark-MXR Inc.) with a pulse duration of 150 fs operating at 1 kHz repetition rate was used. The schematic of the experimental setup is shown in Fig. 1. The original beam was passed through a circular aperture placed in front of the beam delivery system in order to improve the beam quality. The incoming laser beam had a Gaussian profile with a diameter of about 6 mm after magnifying 2 times using a conventional beam expander. The laser beam was subsequently focused using a microscope objective lens (NA = 0.1,

Meiji S.Plan M5X) onto the surface of the specimen which was mounted on a computer controlled x-y translation stage having a resolution of 100 nm. The pulse energy was measured using a photodiode (Ophir, PD300-3W) that was placed after the microscope objective lens and varied using neutral density filters and a linear polarizer. Since the beam diameter cannot be measured precisely, we applied the ablation threshold of Si for multiple laser pulses as a reference point to calculate the beam diameter and the laser fluence because the damage threshold of Si for multiple laser pulses is relatively well defined between 0.18 ~ 0.2 J/cm^2 in the literature [17,21,30]. The single shot ablation threshold of Si was found to be 0.63 J/cm^2 when we applied the damage threshold of 0.2 J/cm^2 for 20 laser pulses as a reference. The specimen was moved at a translation speed, ranging between 10 ~ 100 mm/min in the direction perpendicular to the incident beam.

3. Results and discussion

3.1 Crater formation by single shot

A. Crater depth vs. laser fluence

To understand ablation mechanism from the evolution of surface morphologies, single shots at various laser fluences were irradiated on the Si wafer to create micro-sized craters, and the surface profiles and morphologies were investigated. The measured crater depth, diameter and rim height are plotted as a function of laser fluence in Fig. 1. From the crater depth data shown in Fig. 1(a), it is possible to identify two different ablation regimes having linear dependencies between the ablated depth and the laser fluence on a logarithmic scale. The two different slopes under femtosecond laser irradiation have been reported for metals [26,31], semiconductors [21,32,33], and polymers [34]. The two

regimes are distinguished by the volume over which the laser pulse energy is distributed. These volumes are determined by the optical or heat penetration depth for the low or high fluence regime, respectively. They are described by

$$L_{optical,heat} \cong l_{optical,thermal} \ln \frac{F}{F_{th}^{o,t}}$$

Here, F and F_{th} characterize the applied and threshold fluence, respectively. L is the ablation depth for the two regimes. At low fluence, the number of hot electrons is so low that the charge carriers reach thermal equilibrium with the lattice in a short period time of picoseconds. This short time gives the charge carriers less time to move, which means the optical penetration depth of the laser energy will exceed the thermal diffusion length of the charge carriers, therefore energy transfer occurs only within the volume characterized by the optical penetration depth $l_{optical} = 1/\alpha$. However, for higher fluence, the charge carriers have more energy and it takes longer for them to reach the thermal equilibrium with the lattice. Therefore, electron diffusion length $l_{thermal}$ becomes significant causing an increase in the ablation rate. In this study, an abrupt increase of rim height as shown in Fig. 1(b) was chosen as a separation point between the two regimes. The results of the fit to two separate sets of experimental data are given in Table 1 with the results from the literature for comparison. The results from the current work show fairly good agreement with that of Hwang [19] except for the ablation threshold for high fluence regime. The optical penetration depth was found to be much lower than 10 μm derived from the absorption coefficient of Si at 780 nm [35]. This discrepancy might be attributed to the nonlinear absorption characteristics of femtosecond laser irradiation. The estimated ablation threshold fluence of 0.557 J/cm^2 for low fluence regime can be considered as the minimum fluence for crater formation by a single pulse. Meanwhile, the laser fluence of

1.181 J/cm^2 may be interpretered as the level beyond which the electron temperature that attains a maximum at the target surface near the end of the pulse is sufficiently high to sustain carrier diffusion into the bulk. Figure 2(a) shows typical surface profiles of the craters created at various laser fluences. Based on these surface profiles, the ablated volume of each crater and the ablation efficiency were calculated as a function of laser fluence. Figure 2(b) shows the ablation efficiency and is shown to have the maximum between 10 and 20 J/cm^2 which decreases sharply afterwards. This trend is very similar to the results reported in picosecond laser ablation of copper [36] and in femtosecond micromachining of silicon [19].

B. Surface morphologies

In this study, the surface morphologies of craters produced by single pulses with laser fluences ranging from 0.625 J/cm^2 to 666 J/cm^2 were analyzed using a FESEM and a surface profiler. Based on the morphological observations and topological analysis of the craters, it was possible to categorize them into four characteristic crater patterns as indicated in Fig. 1(b). In the first region near the threshold fluence ($0.557 \leq F < 0.83$ J/cm^2), the crater exhibits different circular regions of ablation, annealing, and modification as shown in Fig. 3(a). It is suggested that the ablation process is generally thermal in nature, and that Coulomb explosion does not take place. For Si, higher electron mobility and higher density of available free electrons ensure effective screening and a much smaller net positive charge accumulation during the laser pulse. This is not sufficient to induce a macroscopic electrostatic breakup of the outer layers of Si [37]. The crater has very smooth surface and there is no rim which protrudes above the Si surface.

This means that there was no formation of plasma at this level of laser fluence. From the second region ($0.83 \leq F < 3.3$ J/cm^2), a circular rim surrounding a smooth center is raised 20 ~ 80 nm above the surface with its height increased linearly with the corresponding increase in the laser fluence. The image (Fig. 3(b)) suggests that the rim is a resolidified splash of molten pool generated during the ablation process. Droplets are not observed beyond the rims of the craters. Ripples, which are formed after irradiation with multiple pulses onto the same sample spot [19,21], are not observed from the surface morphology. Although the energy transfer to Si is determined by the optical penetration depth and a rapid energy transfer occurs only within the volume characterized by the optical penetration depth within this level of fluence, enough energy is still deposited in the undamaged part of the material to create a shallow molten pool below the ablated area. Therefore, force acting on the fluid can drive molten material from the center to the edges of the crater if the melt lifetime is long enough. Because plasma is not formed up to this level of fluence, the only force acting on the molten Si is a thermocapillary force, which is induced by the temperature gradient on the surface following the Gaussian beam intensity profile of the laser. In the third region ($3.3 \leq F < 250$ J/cm^2), crater depth and rim height increases sharply with the increase in laser fluence as the thermal diffusion of the charge carriers becomes dominant. From the laser fluence of 12.5 J/cm^2, different crater morphology with droplets of Si near the outer rim of the crater was observed (Fig. 3(c)), and these droplets became more irregular and reach further from the edge of the rims as the laser fluence increases. This hydrodynamic motion of molten Si is most likely caused by the plasma recoil pressure acting on the molten Si surface. The plasma formation in the ablated plume occurs both from the thermionic electron emission from

the hot surface and from the multiphoton absorption by the plume. The plasma pressure is very high initially and drops to 10 atm during the first microsecond of its expansion [24]. The pressure gradients are particularly large at the edges of the ablated crater because of the plasma/air interface. Because of these large pressure gradients, a very fast rise of a thin rim at the edges of the melted surface is expected. The thin strip-like splashes expanding away from the crater might therefore be a result of very fast rising rims that broke down and resolidified on the surface. As the laser fluence increases further beyond 25 J/cm^2, surface morphologies with the evidence of a violent and explosive removal of molten Si were observed. Another small crater was formed at the center of the crater, and rough recast layers were observed inside the crater and beyond the rim as seen in Fig. 3(d). These crater morphologies appear up to the laser fluence of 125 J/cm^2 (Fig. 3(e)). In the fourth region where the laser fluence exceeds beyond 250 J/cm^2, the crater diameters increase sharply with the increase in the laser fluence, and the surface morphologies reveal a sequential flow of the molten Si as seen in Fig. 3(f). This indicates that there is another driving force which presses down the molten Si layer to produce outward flow of the molten Si. Hwang [19] reported that air breakdown and subsequent strong shock wave envelop were observable from the time-resolved shadowgraphs when the laser fluence exceeded ~ 300 J/cm^2. Therefore, it appears that the femtosecond laser pulse induced air breakdown, followed by the shock wave, is likely to be the driving force to push the molten Si outward and leave such a violent surface morphology.

3.2 Pocket milling by multiple shots

In order to investigate the effect of process parameters on the depth and surface

morphology of a micromilled pocket, the laser fluence, number of passes, and the translation speed were chosen as process parameters, and several sets of pockets (0.4mm × 0.2mm × h) were milled with a scan step of 2 μm. After milling the pockets, the specimens were ultrasonically cleaned with isopropanol for 30 minutes to remove the debris redeposited loosely inside the pockets. Figure 4 shows a series of SEM images of pockets milled at the translation speed of 833 μm/sec at various laser fluences, which illustrates how the surface morphology evolves. As the laser fluence increases, the pocket depth increases, the milled surface becomes rougher due to the thicker resolidified material and debris redeposition, and the striations orthogonal to the translational direction become apparent. The formation of these striations, likely to be initiated from the laser-induced periodic surface structures (LIPSS) [4,19], was observed on a variety of material after irradiation with one or more pulses from a wide range of laser systems (femtosecond, picosecond, and nanosecond pulses). The milled depths were measured using a stylus-type profilometer and are plotted Fig. 5. Figure 5(a) shows the relationship between the laser fluence and the milled depth, which indicates the logarithmic two-regime model observed in the case of single shot craters (Fig. 1(a)) fits well to the multiple-pulse ablation of moving targets. The depths of the pockets as a function of translation speed v for three different laser fluence conditions are graphed in Fig. 5(b). Ameer-Beg[16] and Crawford[20] reported that the groove depth was roughly inversely proportional to the translation speed in the cases of single-pass groove cut of silicon and fused silica. The curve fits to the three sets of data show that the milled depth decays exponentially with increase of the translation speed. This might be due to the incubation effect which has been observed in various materials including semiconductors [30],

leading to an ablation threshold fluence that is strongly affected by the number of pulses incident on the sample. As deep structures are usually milled by applying multiple passes with fixed or varying focal position, the effect of the number of passes on the milled depth and the surface morphology was also investigated. The milled depth has a linear dependency on the number of passes up to 20 as shown in Fig. 5(c), but this linear dependency is deteriorated due to the formation of cone-shaped periodic surface structures as the milled depth becomes deeper. The effect of the process parameters on the roughness was investigated and displayed in Fig. 6. An optimal range of laser fluence for silicon micromilling which results in a better surface roughness is 2~8 J/cm^2. The relationship between the translation speed and the surface roughness is graphed in Fig. 6(b) which shows the same dependency with the milled depth (Fig. 5(a)). Figure 6(c) shows that the surface roughness gradually increases with the increase in the number of passes, and that the laser fluence has a strong effect on the surface roughness. Figure 7 illustrates the evolution of the surface morphologies of the pockets milled with various numbers of passes at the translation speed of 50 mm/min. After 2 passes, the bottom surface of uniformly milled pocket showed a periodic trace of laser raster (2 μm period) and small irregular structures form the initial stage of periodic cone-shaped features, the periodic structures become more ordered and larger as the number of passes increases. The formation of the cone-shaped structures has the same trend up to the laser fluence of ~ 25 J/cm^2, the periodic structures become larger and taller with the increase of laser fluence as shown in Fig. 8. These results suggest that the lateral and vertical extension of the cone-shaped structures and the spacing between them strongly depends on the laser fluence and the number of pulses incident on the sample. The formed cone-shaped

structures seem to have an elliptic base, with the longer axis of the ellipse perpendicular to the polarization axis of the incident light. Recently, Tull [38] suggested a formation mechanism of the silicon microstructures (columns and cones) based on the explanation of Bonse [19] and Lowndes [39]. At the early stage (1-10 pulses), a LIPSS-like ripple pattern with a wavelength of the laser appears, and then changes to a quasi-periodic array of beads with a larger wavelength. During the late-stage, from 10 to several hundred pulses, ablation takes place preferably on the sides of these beads. The beads act to concentrate the light into the valley between them. Light that hits the sides of the beads has a high angle of incidence, and the absorbed local laser fluence is reduced due to high reflectivity. This light is reflected into the valleys, raising the incident fluence and increasing the ablation rate. As the conical structures become steeper, the effect is intensified. As the laser fluence increases above 25 J/cm^2, the micromilled pockets showed completely different surface morphologies, the surface is covered with thick resolidified material and quasi-periodic holes appear at the bottom of the pockets as shown in Fig. 9. This dramatic change might be attributed to the violent and explosive removal of molten silicon observed in Fig. 3(d). Figure 10 displays the milling efficiency as a function of the laser fluence. The milling efficiency is defined as the milled depth per unit laser fluence, it is shown to have the same trend with the single pulse ablation efficiency (Fig. 2(b)), with the maximum efficiency lies between 10 and 20 J/cm^2.

4. Conclusion

We have investigated the micromilling of silicon surfaces with femtosecond laser. The morphological observation and geometric analysis of the craters created by single-shot

irradiation indicated that the material removal is thermal in nature and there are two distinct ablation regimes of low and higher fluence with logarithmic relationship between the ablation depth and the laser fluence. The surface morphologies revealed the thermodynamic and hydrodynamic motion of the molten silicon played a key role in the material removal and the crater formation. Crater patterns were categorized into four characteristic groups and their formation mechanisms were investigated. Femtosecond laser micromilling of pockets in silicon was systematically performed for the first time to explore the effect of the process parameters such as pulse energy, translation speed, and the number of passes on the material removal and the surface morphology. The milled depth and the surface roughness have strong relations with the process parameters. The surface morphologies showed the evolution of periodic cone-shaped structures having elliptic bases with the longer axis of the ellipse perpendicular to the polarization axis. The periodic microstructures become more ordered and bigger as the number of passes increases and become bigger and taller with the increase in the laser fluence.

Femtosecond laser micromilling of silicon requires further study to define effective process windows for new application areas. Although the micromilled pockets have characteristic microstructured surface finish and it could limit its applications, its advantages such as the high dimensional accuracy, depth controllability, and flexible machining show the potential as an alternative to conventional photolithography based processes.

Acknowledgements

The authors would like to acknowledge Mahmud Islam, Director, Precision and

Freeform Fabrication Technologies, for his support. Thanks are also due to Hugo Reshef, Marco Zeman, and Matthew Shiu for their technical assistance.

References

[1] D. Bauerle: Laser Processing and Chemistry, 3rd Ed. (Springer-Verlag, Berlinm 2000)

[2] B.N. Chichkov, C. Momma, S. Nolte, F. von Alvensleben, A. Tummermann, Appl. Phys, A **63**, 109 (1996)

[3] S. S. Mao, F. Quere, S. Guizard, X. Mao, R. E. Russo, G. Petite, P. Martin, Appl. Phys. A. **79,** 1695 (2004)

[4] D.V. Tran, Y.C. Lam, H.Y. Zheng, V.M. Murukeshan, J.C. Chai, D.E. Hardt, International Conference on Precision Engineering, 2004, Singapore, Mar 2-5, pp. 265-272, (2004)

[5] C.V. Shank, R. Yen, C. Hirlimann, Phys. Rev. Lett. **50**, 454 (1983)

[6] A. Cavalleri, K. Slkolowski-Tinten, J. Bialkoski, M. Schreiner, D. von der Linde, J. Appl. Phys. **85**, 3301 (1999)

[7] A.V. Bulgakov, I. Ozerov, W. Marine, Appl. Phys. A **79**, 1591 (2004)

[8] P.P. Pronko, P.A. VanRompay, C. Horvath, F. Loesel, T. Juhasz, X. Liu, G. Mourou, Phys. Rev. B **58**, 2387 (1998)

[9] W.G. Roeterdink, N.B.F. Juurlink, O.P.H. Vaughan, J. Dura Diez, M. Bonn, Appl. Phys. Lett. **82**, 4190 (2003)

[10] D. von der Linde, K. Slkolowski-Tinten, Appl. Surf. Sci. **154**, 1 (2000)

[11] X. Xu, C. Cheng, I.H. Chowdhury, J. of Heat Transfer **126**, 727 (2004)

[12] H. Ki, J. Mazumder, J. of Las. Appl. **17**, 110 (2005)

[13] R. Holenstein, S.E. Kirkwood, R. Fedosejevs, Y.Y. Tsui, Proceedings of the SPIE Vol. **5579**, 688 (2004)

[14] B. Tan, K. Venkatakrishnan. J. of Micromech. Microeng. **16**, 1080 (2006)

[15] F. Costache, S. Kouteva-Arguirova, J. Reif, Appl. Phys. A **79**, 1429 (2004)

[16] S. Ameer-Beg, W. Pierre, S. Rathbone, J. Wright, W. Weaver, H. Champoux, Appl. Surf. Sci. **127-129**, 875 (1998)

[17] J. Bonse, S. Baudach, J. Kruger, W. Kautek, M. Lenzner, Appl. Phys. A **74**, 19 (2002)

[18] R. Le Harzic, Opt. Exp. **13**, 6651 (2005)

[19] D.J. Hwang, C.P. Grigoropoulos, J. of Appl. Phys. **99**, 083101 (2006)

[20] T.H.R. Crawford, A. Borowiec, H.K. Haugen, Appl. Phys. A **80**, 1717 (2005).

[21] E. Coyne, J.P. Magee, P. Mannion, G. O'Connor, SPIE Vol. **4876**, 487 (2003)

[22] D.T. Pham, S.S. Dimov, C. Ji, P.V. Petkov, T. Dobrev, Proc. Inst. Mechanical Engineers, J. of Eng. Manuf. **218 Part B**, 1 (2004)

[23] D. Karnakis, G. Rutterford, M. Knowles, T. Dobrev, P. Petkov, S. Dimov, Proc. of SPIE Vol. **6106**, 610604 (2006)

[24] A. Ben-Yakar, R.L. Byer, Appl. Phys. Lett. **83**, 3030 (2003)

[25] J. Zhao, B. Huettner, A. Menschig, Opt. & Las. Technol. **33**, 487 (2001)

[26] C. Momma, S. Nolte, B.N. Chichkov, F.v. Alvensleben, A. Tunnermann, Appl. Surf. Sci. **109/110**, 15 (1997)

[27] A. Malshe, D. Deshpande, E. Stach, K. Rajurkar, D. Alexander, Annals of the CIRP, 53/1, (2004)

[28] E. Coyne, J.P. Magee, P. Mannion, G. O'Connor, T.J. Glynn, Appl. Surf. Sci. **229**, 148 (2004)

[29] H. Huang, H.Y. Zheng, G.C. Lim, Appl. Surf. Sci. **228**, 201 (2004)

[30] N. Uppal, P.S. Shiakolas, S. Priya, Ferroelectric Letters **32**, 67 (2005)

[31] K. Furusawa, K. Takahashi, H. Kumagai, K. Midorikawa, M. Obara, Appl. Phys. A: Mater. Sci. Process. **69**, S359 (1999)

[32] S. Besner, J.Y. Degorce, A.V. Kabashin, M. Meunier, Appl. Surf. Sci. **247**, 163 (2005)

[33] M.I. Park, C.S. Kim, C.O. Park, S.C. Jeong, Opt. and Las. In Eng. **43**, 1322 (2005)

[34] Z.B. Wang, M.H. Hong, Y.F. Lu, D.J. Wu, B. Lan, T.C. Chong, J. of Appl. Phys. **93**, 6375 (2003)

[35] L. Werner, J. Fischer, U. Johannsen, and J. Hartmann, Metrologia Vol. **37**, 279-284 (2000)

[36] S.S. Mao, X. Mao, R. Greif, R.E. Russo, Appl. Phys. Lett. **76**, 31 (2000)

[37] R. Stoian, A. Rosenfeld, D. Ashkenasi, I.V. Hertel, Phys. Rev. Lett. **88**, 097603 (2002)

[38] B.R. Tull, J.E. Carey, E. Mazur, J.P. McDonald, S.M. Yalisove, MRS Bulletin **31**, 626 (2006)

[39] D.H. Lowndes, J.D. Fowlkes, A.J. Pedraza, Appl. Surf. Sci. **154/155**, 647 (2000)

List of Table

List of Fugures

Table 1 Comparison between the parameters estimated from the current and the literature values

		Experimental	Reference [19]
Low Fluence Regime	$l_{optical}$	135 nm	145 nm
	$F_{th}^{(o)}$	0.557 J/cm^2	0.458 J/cm^2
Higher Fluence Regime	$l_{thermal}$	324 nm	322 nm
	$F_{th}^{(t)}$	1.181 J/cm^2	0.657 J/cm^2

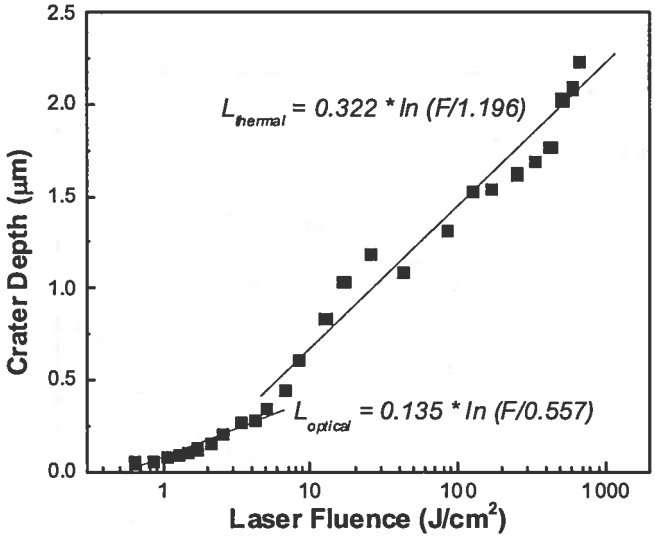

(a)

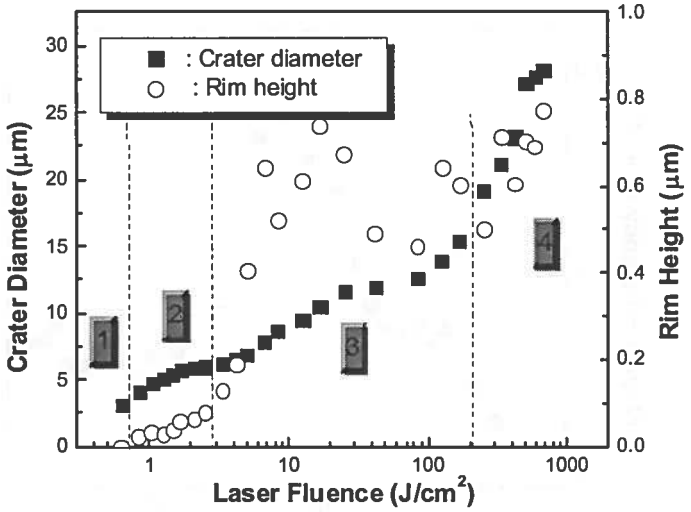

(b)

Fig. 1 (a) Crater depth vs. laser fluence, (b) Crater diameter and rim height vs. laser fluence

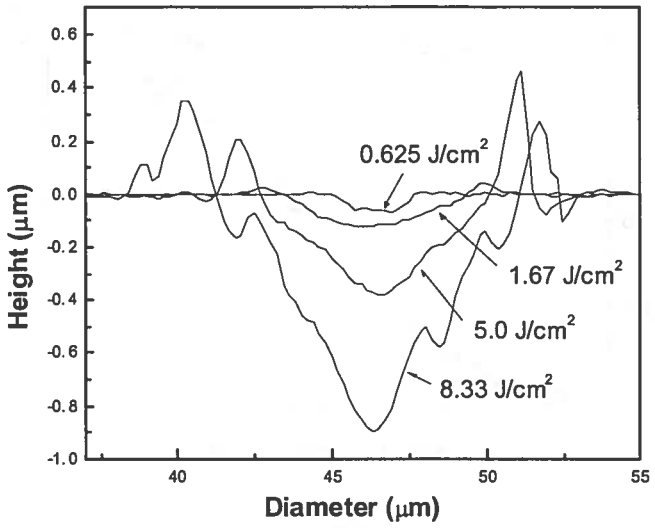

(a)

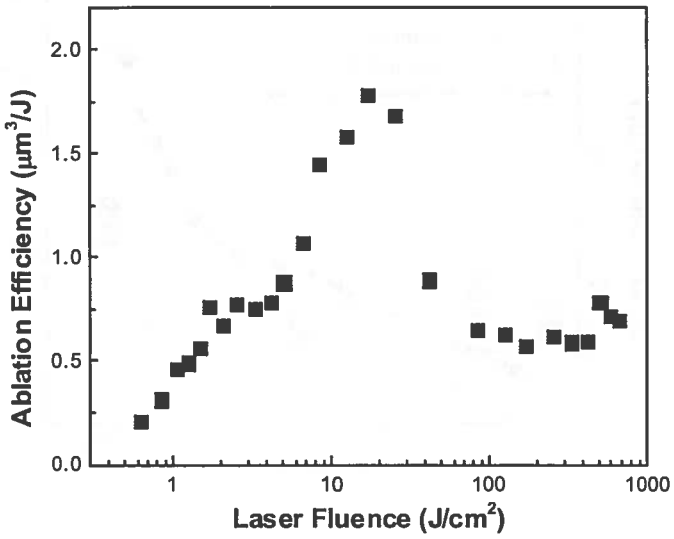

(b)

Fig. 2 (a) Measured surface profiles of the craters, (b) The variation of ablation efficiency with laser fluence

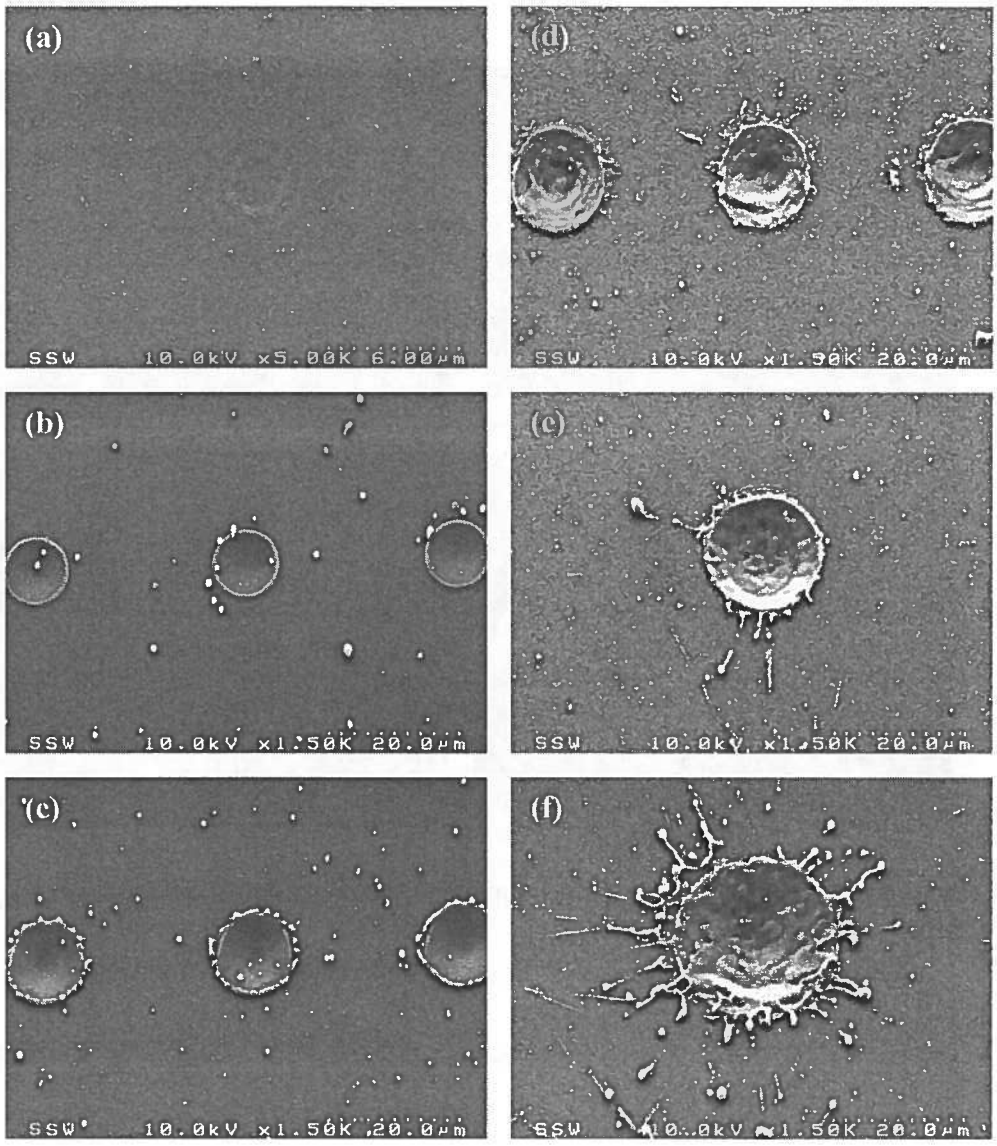

Fig. 3 SEM micrographs of single-shot ablation craters showing characteristic patterns;

(a) F = 0.63 J/cm^2, (b) F = 3.3 J/cm^2, (c) F = 12.5 J/cm^2, (d) F = 25 J/cm^2,

(e) F = 125 J/cm^2, (f) F = 250 J/cm^2

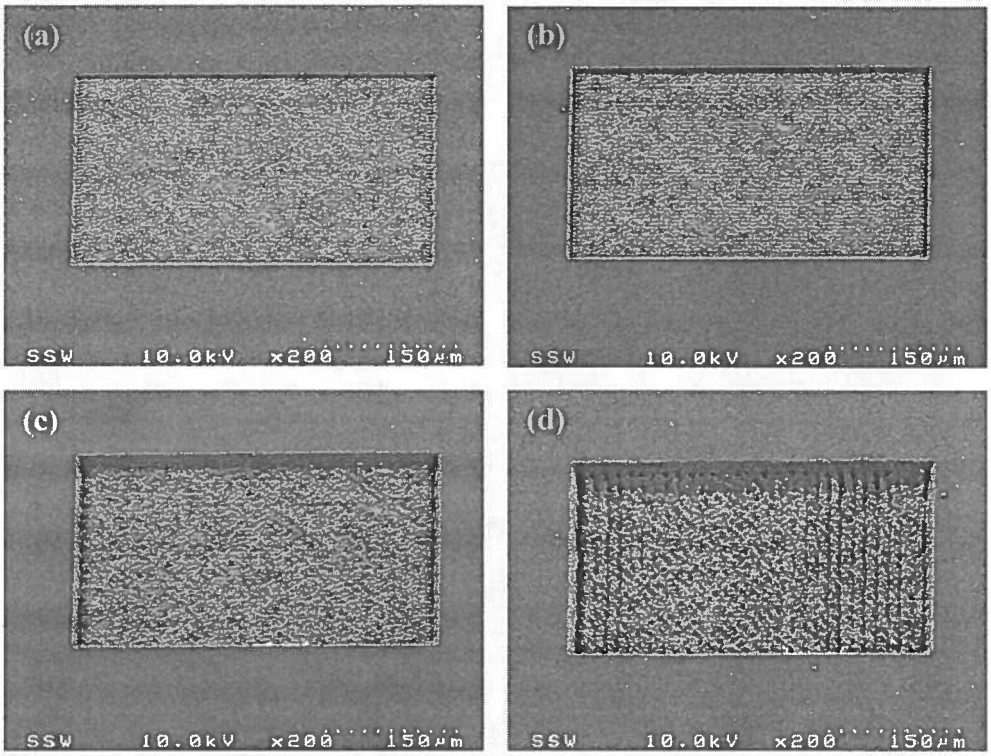

Fig. 4 SEM micrographs showing the effect of laser fluence on the surface structures (laser scan step s = 2 μm, v = 50 mm/min);

(a) F = 1.88 J/cm^2, (b) F = 3.76 J/cm^2, (c) F = 12.5 J/cm^2, (d) F = 25.0 J/cm^2

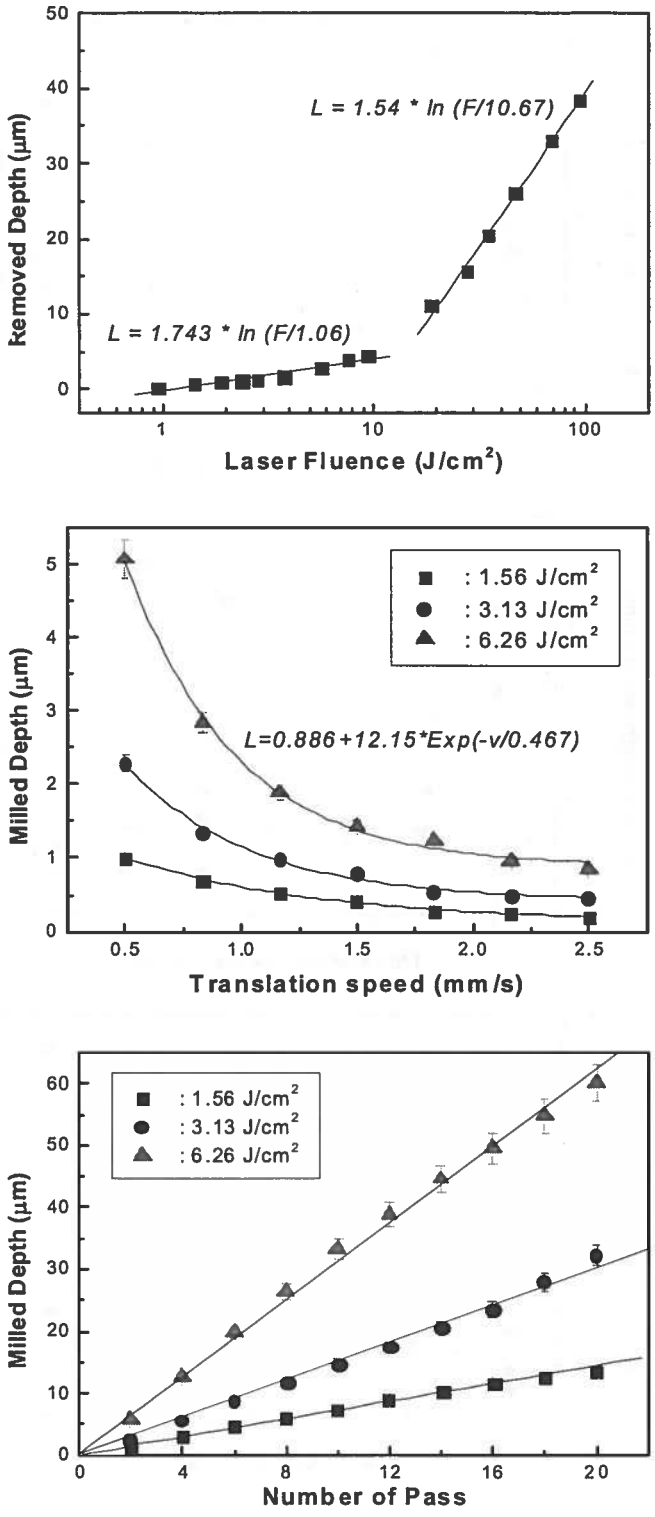

Fig. 5 The relationships between the milled depth and the process parameters;

(a) laser fluence, (b) translation speed, (c) number of passes

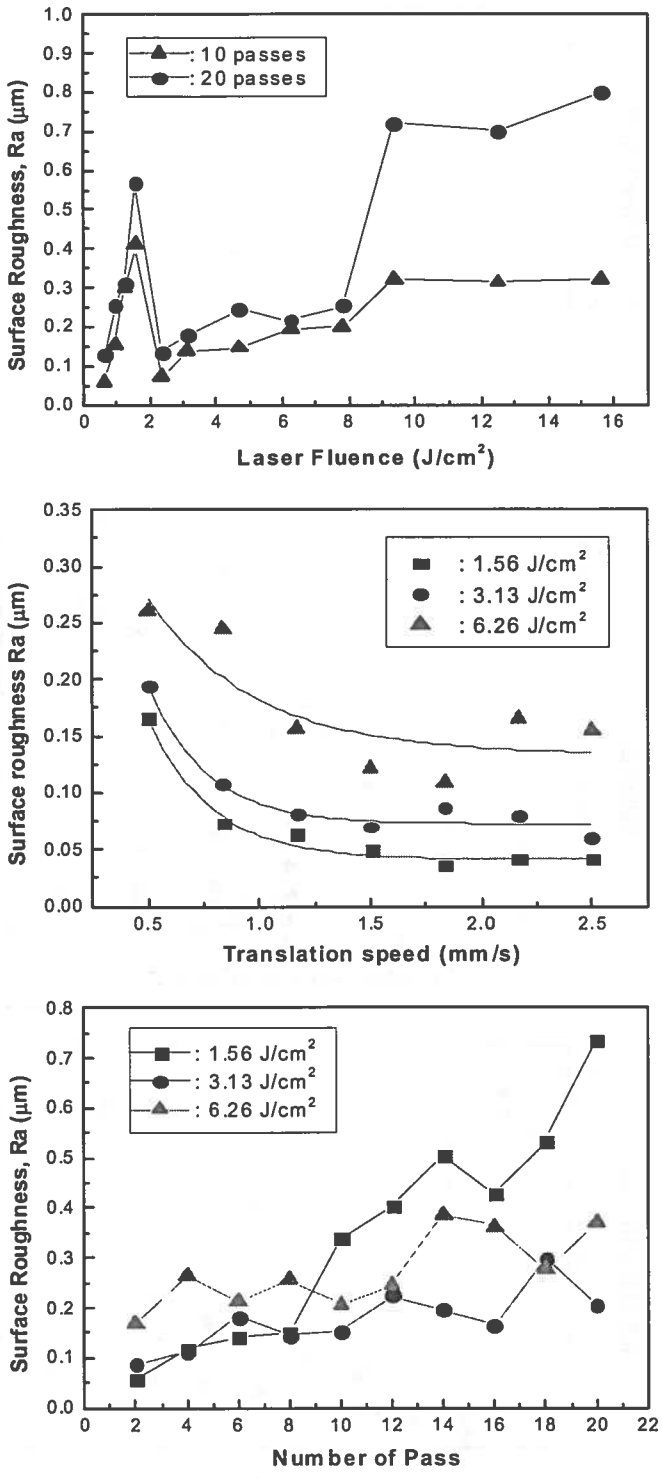

Fig. 6 The relationships between the surface roughness and the process parameters;

(a) laser fluence, (b) translation speed, (c) number of passes

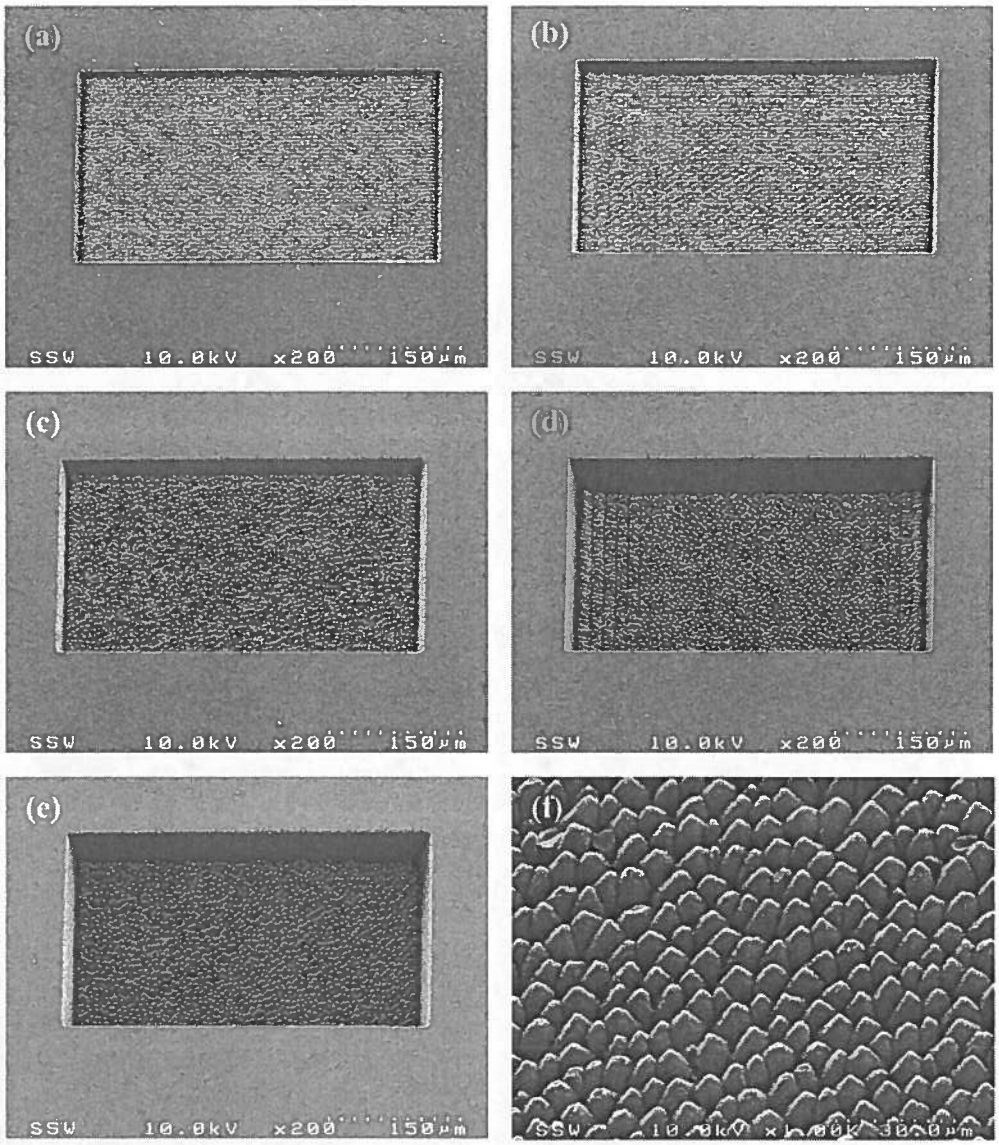

Fig. 7 SEM micrographs showing the evolution of surface structures with the increase in the number of passes (F = 5.0 J/ cm^2, v = 50 mm/min, s = 2 μm); (a) N = 2, (b) N = 6, (c) N = 10, (d) N = 20, (e) N = 30, (f) magnified image of (e)

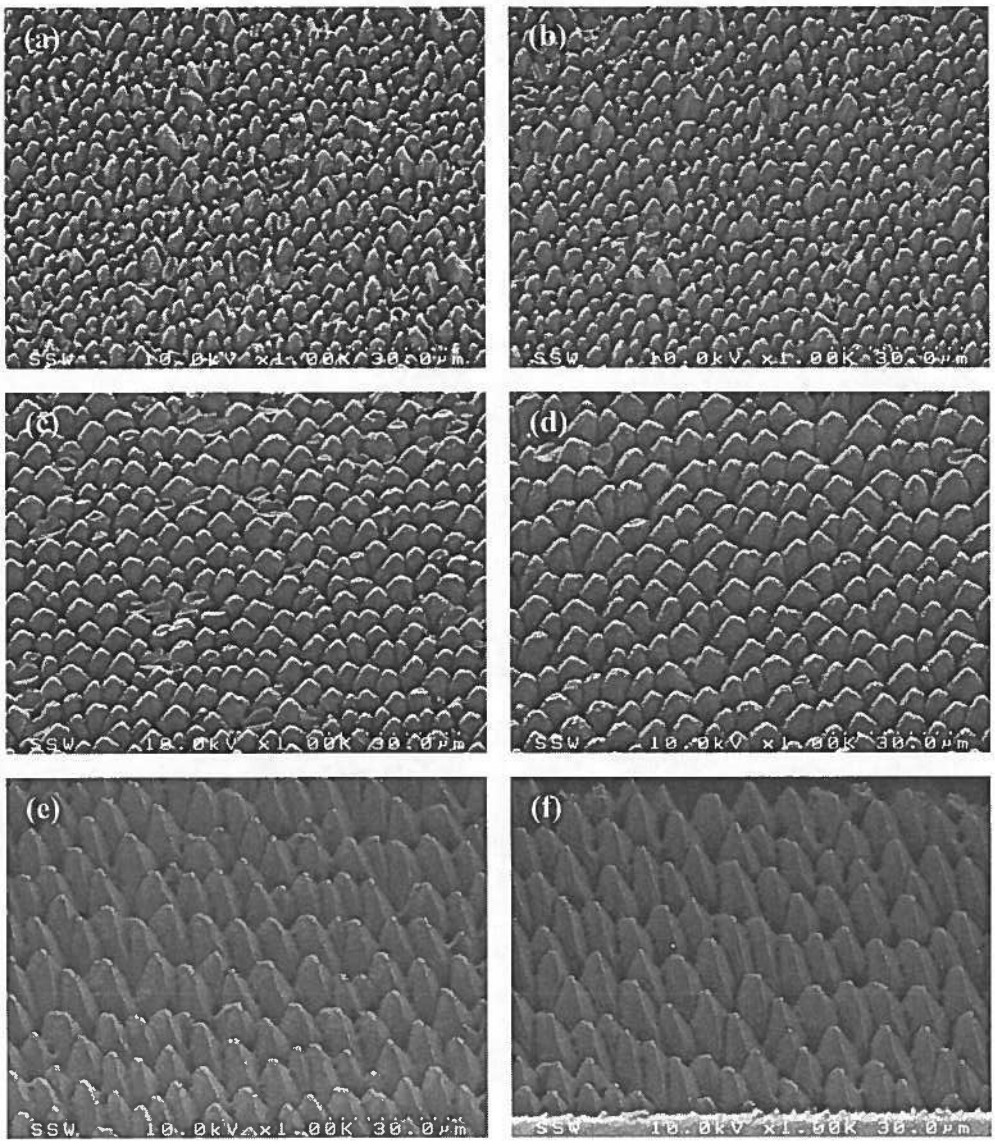

Fig. 8 SEM micrographs showing the fully grown microcone structures after 30 passes; (a) F = 1.25 J/cm^2, (b) F = 1.88 J/cm^2, (c) F = 3.76 J/cm^2, (d) F = 5.0 J/cm^2, (e) F = 12.5 J/cm^2, (f) F = 25.0 J/cm^2

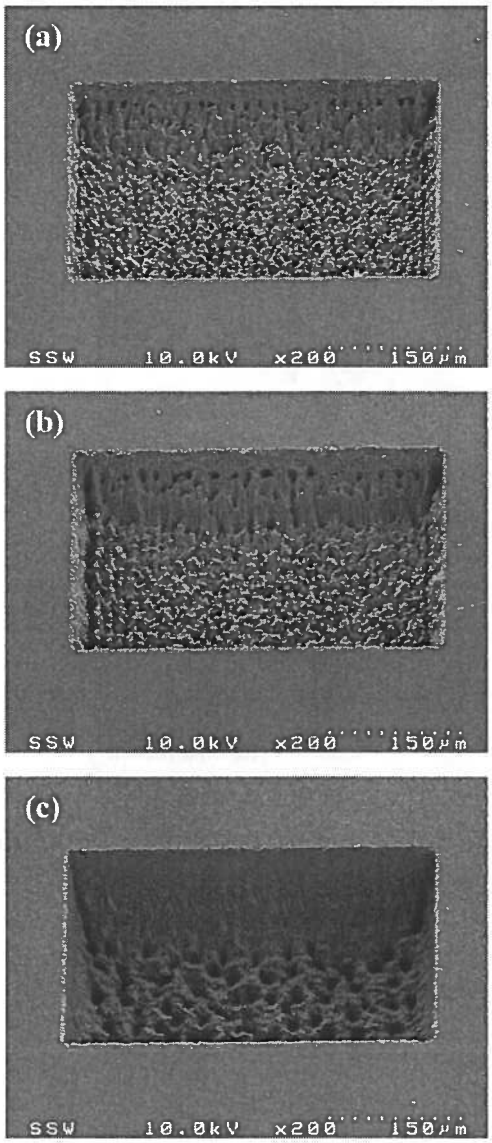

Fig. 9 SEM micrographs showing the evolution of surface structures with the variation of number of passes (F = 62.0 J/cm^2, v = 50 mm/min, s = 2 μm); (a) N = 2, (b) N = 6, (c) N = 10

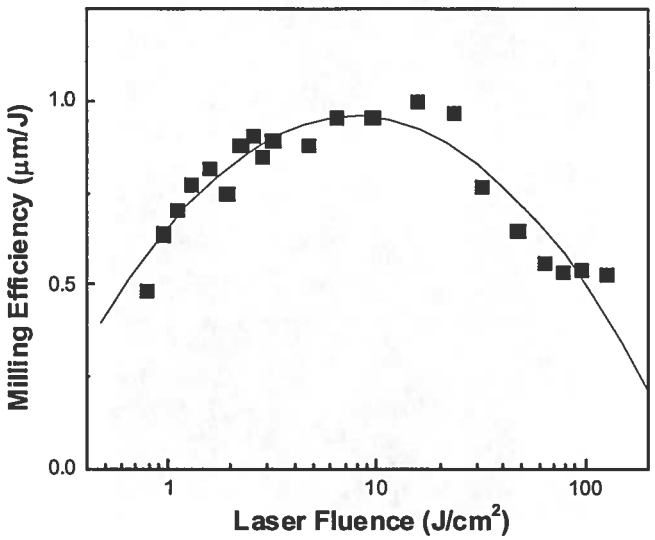

Fig. 10 The variation of micromilling efficiency with laser fluence